

Microscopic optical potentials including breakup effects for elastic scattering

Shoya Ogawa,^{1,*} Ryo Horinouchi,^{1,†} Masakazu Toyokawa,^{1,‡} and Takuma Matsumoto^{1,§}

¹*Department of Physics, Kyushu University, Fukuoka 819-0395, Japan*

(Dated: April 23, 2019)

We construct a microscopic optical potential including breakup effects for elastic scattering of weakly-binding projectiles within the Glauber model, in which a nucleon-nucleus potential is derived by the g -matrix folding model. The derived microscopic optical potential is referred to as the eikonal potential. For d scattering, the calculation with the eikonal potential reasonably reproduces the result with an exact calculation estimated by the continuum-discretized coupled-channels method. As the properties of the eikonal potential, the inaccuracy of the eikonal approximation used in the Glauber model is partially excluded. We also analyse the ${}^6\text{He}$ scattering from ${}^{12}\text{C}$ with the eikonal potential and show its applicability to the scattering with many-body projectiles.

I. INTRODUCTION

Microscopic understanding of nucleon-nucleus (NA) and nucleus-nucleus (AA) optical potentials is one of the most important issues in nuclear reaction theory. The optical potentials are necessary to describe not only elastic scattering but also reactions including higher-order processes. For example, the distorted-wave Born approximation and the continuum-discretized coupled-channels method (CDCC) [1–3] require the optical potentials between constructs of a projectile (P) and a target (T) to describe inelastic scattering, breakup and transfer reactions.

The g -matrix folding model has been widely used as a reliable method to describe the optical potential [4–9]. The g matrix is an effective nucleon-nucleon interaction [10–20] in nuclear matter, and depends on the density ρ_m of the nuclear matter. In the g -matrix folding model, the optical potentials are derived by folding the g -matrix with the target density ρ_T for NA scattering, and with ρ_T and the projectile one ρ_P for AA scattering. The procedures are referred to as the single-folding (SF) model for NA scattering and double-folding (DF) model for AA scattering, respectively.

In the SF model, ρ_T is referred as ρ_m in the g matrix with the local density approximation, and the calculated NA optical potential becomes nonlocal by taking into account knock-on exchange processes. The nonlocal potential is not practical in many applications, but can be localized by the Brieva-Rook approximation [12] in good accuracy. The localized potential is quite successful in reproducing experimental data systematically, when reliable g matrices such as Melbourne [17], CEG [15, 19], and χEFT [20] g matrices are adopted.

On the other hand, it is more difficult to derivate the

optical potential with the DF model for AA scattering than that with the SF model for NA scattering. The main problem of the DF model is how to treat ρ_m in the g matrix for AA scattering. In general, the frozen-density approximation (FDA) is applied, in which the sum of ρ_P and ρ_T is taken as ρ_m in the g matrix. The optical potential derived by the DF model with the FDA often needs a normalization factor for the real and imaginary parts to reproduce experimental data. Thus the choice of ρ_m in the g matrix for the DF model is a longstanding open problem.

In the previous works for ${}^{3,4}\text{He}$ scattering on various targets [21, 22], we proposed the target-density approximation (TDA) in the DF model, where ρ_m is estimated with only ρ_T . The DF model with the TDA (the DF-TDA model) well reproduces experimental data for ${}^{3,4}\text{He}$ scattering with no adjustable parameter, and its theoretical validity can be confirmed by using multiple scattering theory [23–25]. Furthermore, as a practical model of the DF-TDA model, we also proposed the double-single folding (DSF) model for ${}^{3,4}\text{He}$ scattering, in which the optical potential between ${}^{3,4}\text{He}$ and the target is derived by folding the localized NA optical potential of the SF model with the ${}^{3,4}\text{He}$ densities.

However, the optical potential calculated by the DSF model is not taken into account breakup effects on the elastic scattering. In fact, results with the DSF model are slightly different from the experimental data for ${}^3\text{He}$ scattering at low incident energies [22], where breakup effects are important. The discrepancy can be solved by applying the CDCC calculation that can describe breakup effects accurately. CDCC has been successful in analyses of scattering of weakly-binding two- and three-body projectiles. Although CDCC is a reliable method to analyze breakup reactions, it is hard to apply CDCC to scattering of more than four-body projectiles such as ${}^8\text{He}$, because of a high computational cost.

As another approach to describe excitation effects of P and T, the Glauber model [26] has been applied to analyses of AA scattering at intermediate energies. In the Glauber model, nucleon degrees of freedom of P and T are treated by the adiabatic approximation and

*s-ogawa@phys.kyushu-u.ac.jp

†horinouchi@phys.kyushu-u.ac.jp

‡toyokawa@phys.kyushu-u.ac.jp

§matsumoto@phys.kyushu-u.ac.jp

the eikonal approximation. One of advantages of the Glauber model is to construct the optical potential including multiple-scattering effects from the phase-shift function [26–28]. The derived optical potential is called the eikonal potential. Although the eikonal potential has been used to analyses of scattering of weakly-binding projectiles in the previous works [27, 28], the validity of the eikonal potential for incident energies and its property have never been clarified.

In this paper, we investigate the validity of the eikonal potential compared with results of CDCC with the SF model for d scattering at 20–200 MeV/nucleon, which is described by a $p + n + T$ three-body model. The optical potentials for p -T and n -T systems are derived by the SF model with the Melbourne g matrix. Furthermore, in order to discuss the applicability of the eikonal potential to many-body systems, we adopt the eikonal potential to analyses of ${}^6\text{He}$ scattering that is described by a ${}^4\text{He} + n + n + T$ four-body model.

The paper is organized as follows. In Sec. II, we describe the theoretical framework to derive the eikonal potential for d scattering. In Sec. III, numerical results are shown, and properties of the eikonal potential are discussed. Finally, we give a summary in Sec. IV.

II. THEORETICAL FRAMEWORK

A. Glauber model

We consider d scattering on T by a $p + n + T$ three-body model. Note that the below formulation can be easily extend to a three-body projectile system such as scattering of ${}^6\text{He}$ described by a ${}^4\text{He} + n + n + T$ four-body model. The scattering is described by the three-body Schrödinger equation

$$\left[-\frac{\hbar^2}{2\mu} \nabla_{\mathbf{R}}^2 + U(\mathbf{r}, \mathbf{R}) + h_d - E \right] \Psi(\mathbf{r}, \mathbf{R}) = 0, \quad (1)$$

where \mathbf{R} and μ are the relative coordinate and the reduced mass of the d -T system, respectively. The potential U between d and T is represented by

$$U(\mathbf{r}, \mathbf{R}) = U_n(\mathbf{r}, \mathbf{R}) + U_p(\mathbf{r}, \mathbf{R}) + V_C(R), \quad (2)$$

where U_n (U_p) is the optical potential between n (p) and T. In the present analysis, we neglect Coulomb breakup processes, and the the Coulomb potential V_C thus depends on only R . As the internal Hamiltonian h_d for d , we adopt a simple form with the Ohmura potential between p and n [29].

Initially, d is the ground state, and has $\hbar\mathbf{K}$ as the relative momentum according to R at $Z = -\infty$, where Z is the z -axis component of \mathbf{R} , and \mathbf{K} is set to be parallel to Z . Under this initial condition, Ψ is represented by

$$\Psi(\mathbf{r}, \mathbf{R}) \xrightarrow[Z \rightarrow -\infty]{} e^{i\mathbf{K}Z + \dots} \Phi_0(\mathbf{r}), \quad (3)$$

where the “ \dots ” represents effects of the Coulomb distortion. The ground state wave function Φ_0 of d satisfies

$$h_d \Phi_0(\mathbf{r}) = \epsilon_0 \Phi_0(\mathbf{r}), \quad (4)$$

and the total energy conservation is defined as

$$\frac{\hbar^2 K^2}{2\mu} = E - \epsilon_0 \equiv E_0. \quad (5)$$

The Glauber model is based on the adiabatic approximation and the eikonal approximation. In the adiabatic approximation, h_d in Eq. (1) is replaced by ϵ_0 . In the eikonal approximation, Ψ is described as the product of a plane wave by a new function $\hat{\Psi}$,

$$\Psi(\mathbf{r}, \mathbf{R}) = e^{i\mathbf{K}Z} \hat{\Psi}(\mathbf{r}, \mathbf{R}). \quad (6)$$

Inserting Eq. (6) into Eq. (1) with the adiabatic approximation, the equation for $\hat{\Psi}$ is obtained as

$$\left[-\frac{\hbar^2}{2\mu} \nabla_{\mathbf{R}}^2 - i\hbar v \frac{\partial}{\partial Z} + U(\mathbf{r}, \mathbf{R}) \right] \hat{\Psi}(\mathbf{r}, \mathbf{R}) = 0, \quad (7)$$

where $v = \hbar K/\mu$. As an essence of the eikonal approximation, the second derivatives of $\hat{\Psi}$ for \mathbf{R} is neglected by assuming that $\hat{\Psi}$ varies smoothly with \mathbf{R} . Accordingly, Eq. (7) is rewritten as

$$i\hbar v \frac{\partial}{\partial Z} \hat{\Psi}(\mathbf{r}, \mathbf{R}) = U(\mathbf{r}, \mathbf{R}) \hat{\Psi}(\mathbf{r}, \mathbf{R}). \quad (8)$$

The conditions for the accuracy of the eikonal approximation are well known as

$$\frac{|U|}{E_0} \ll 1, \quad a_U K \gg 1, \quad (9)$$

where a_U is the radius of U .

If U does not include V_C , Eq. (8) can be solved analytically under the initial condition as

$$\hat{\Psi}(\mathbf{r}, \mathbf{R}) = \exp \left[-\frac{i}{\hbar v} \int_{-\infty}^Z U(\mathbf{r}, \mathbf{b}, Z') dZ' \right] \Phi_0(\mathbf{r}), \quad (10)$$

where \mathbf{b} is the projection of \mathbf{R} onto the x - y plane. In the eikonal approximation, the elastic scattering amplitude is given by

$$f_{\text{el}}(\mathbf{q}) = \frac{iK}{2\pi} \int d\mathbf{b} e^{-i\mathbf{q}\cdot\mathbf{b}} [1 - \mathcal{S}(\mathbf{b})], \quad (11)$$

where the forward-scattering approximation is adopted, and \mathbf{q} is the transfer momentum. The eikonal S matrix, \mathcal{S} , is defined as

$$\mathcal{S}(\mathbf{b}) = \langle \Phi_0 | e^{i\chi(\mathbf{r}, \mathbf{b})} | \Phi_0 \rangle \quad (12)$$

with the phase-shift function

$$\chi(\mathbf{r}, \mathbf{b}) = -\frac{1}{\hbar v} \int_{-\infty}^{\infty} U(\mathbf{r}, \mathbf{R}) dZ. \quad (13)$$

This expression is valid for U without V_C . When U includes V_C , we need a special treatment because of the well-known logarithmic divergence of χ .

To describe scattering with the Coulomb interaction in the Glauber model, various approaches have been proposed so far. In this study, we apply the simplest way with the sharp cut screened Coulomb potential with the cut off radius a_C , and the elastic scattering amplitude is thus rewritten as

$$f_{\text{el}}^G(\mathbf{q}) = [f_{\text{Ruth}}(\mathbf{q}) + f_N(\mathbf{q})] e^{-2i\eta \ln(2ka_C)}, \quad (14)$$

where f_{Ruth} is the the Rutherford amplitude and η is the Zommerfeld parameter. f_N represents the nuclear part of the scattering amplitude given by

$$f_N(\mathbf{q}) = \frac{iK}{2\pi} \int d\mathbf{b} e^{-i\mathbf{q}\cdot\mathbf{b}+2i\eta \ln(kb)} [1 - \mathcal{S}_N(\mathbf{b})] \quad (15)$$

with the nuclear part of the eikonal S matrix

$$\mathcal{S}_N(\mathbf{b}) = \langle \Phi_0 | e^{i\chi_N(\mathbf{r},\mathbf{b})} | \Phi_0 \rangle \quad (16)$$

and the phase-shift function

$$\chi_N(\mathbf{r}, \mathbf{b}) = -\frac{1}{\hbar v} \int_{-\infty}^{\infty} [U_n(\mathbf{r}, \mathbf{R}) + U_p(\mathbf{r}, \mathbf{R})] dZ. \quad (17)$$

Here it should be noted that although f_{el} of Eq. (14) depends on a_C , the differential cross section defined as $|f_{\text{el}}^G(\mathbf{q})|^2$ does not depend on a_C . In this paper, we refer to the calculation with $f_{\text{el}}^G(\mathbf{q})$ as the Glauber model.

B. Eikonal potential model

According to the approach proposed by Glauber, we can derive the local optical potential U_{opt} in the following. First, we introduce a new phase-shift function $\tilde{\chi}_N$ to reproduce \mathcal{S}_N obtained from Eqs. (16) and (17);

$$\mathcal{S}_N(b) = e^{i\tilde{\chi}_N(b)}. \quad (18)$$

Here it should be noted that \mathcal{S}_N depends on only $b = |\mathbf{b}|$ since U_n and U_p are taken into account only the central parts as mentioned later. Then we assume that $\tilde{\chi}_N$ is described by the local and spherical optical potential U_E as

$$\tilde{\chi}_N(b) = -\frac{1}{\hbar v} \int_{-\infty}^{\infty} U_E(R) dZ. \quad (19)$$

Finally, Solving Eq. (19) for U_E , we obtain the following form

$$U_E(R) = \frac{\hbar v}{\pi} \frac{1}{R} \frac{d}{dR} \int_R^{\infty} b db \frac{\tilde{\chi}_N(b)}{\sqrt{b^2 - R^2}}. \quad (20)$$

The details for derivation of U_E are shown in Refs. [26–28]. In this paper, the calculation with U_E is called the eikonal potential model (the EP model), in which the

two-body Schrödinger equation for d -T scattering is defined as

$$\left[-\frac{\hbar^2}{2\mu} \nabla_{\mathbf{R}}^2 + U_E(R) + V_C(R) - E_0 \right] \Psi_{\text{EP}}(\mathbf{R}) = 0. \quad (21)$$

Here it should be noted that U_E includes breakup effects of d through the Glauber model. Meanwhile, the optical potential in the DSF model (DSF potential) is defined as

$$U_{\text{DSF}}(R) = \langle \Phi_0 | U_n(\mathbf{r}, \mathbf{R}) + U_p(\mathbf{r}, \mathbf{R}) | \Phi_0 \rangle, \quad (22)$$

in which breakup effects of d are not taken into account.

C. NA optical potential

In the present analysis, we derive U_n and U_p by the g -matrix folding model. In the g -matrix folding model, the optical potential is obtained by folding the g matrix with the target density, and the knock-on exchange processes between the interacting two nucleons are considered as the dominant component of the antisymmetrization [30, 31]. The folding potential is generally nonlocal because of the knock-on exchange process, but the nonlocality is well localized by the Brieva-Rook method [12]. The folding potential is composed of the direct (DR) and exchange (EX) terms

$$U_j(R_j) = U_j^{\text{DR}}(R_j) - U_j^{\text{EX}}(R_j) \quad (23)$$

where $j = n$ or p , and R_j is the relative coordinate between particle j and T. Each term is written with the one-body and mixed densities, ρ_T and $\tilde{\rho}_T$, as

$$U_j^{\text{DR}}(R_j) = \sum_{\nu} \int d\mathbf{r}_T g_{j\nu}^{\text{DR}}(s, \rho) \rho_T^{(\nu)}(\mathbf{r}_T), \quad (24)$$

$$U_j^{\text{EX}}(R_j) = \sum_{\nu} \int d\mathbf{r}_T g_{j\nu}^{\text{EX}}(s, \rho) \tilde{\rho}_T^{(\nu)}(\mathbf{r}_T, \mathbf{R}_j) j_0(K(R_j)s). \quad (25)$$

Here the index ν represents the z -component of isospin of the nucleons in T, \mathbf{r}_T is the internal coordinate of T, and $\mathbf{s} = \mathbf{r}_T - \mathbf{R}_j$. The g matrix $g^{\text{DR(EX)}}$ is the direct (exchange) term of the g matrix among the considering nucleons. The mixed density can be described by using the one-body density with the local Fermi gas approximation [32] as

$$\tilde{\rho}_T(\mathbf{r}_T, \mathbf{R}_j) = \rho_T(|\mathbf{r}_T - \mathbf{s}/2|) \frac{3j_1(k_F^T s)}{k_F^T s}. \quad (26)$$

In the present study, we employ the Melbourne g matrix [17] constructed from Bonn-B nucleon-nucleon interaction [33]. The Melbourne g matrix well reproduce nucleon elastic scattering with and without localization of the exchange term [17, 34]. For ^{208}Pb , the matter density is calculated by the spherical Hartree-Fock method with the Gogny-D1S interaction [35] and the spurious

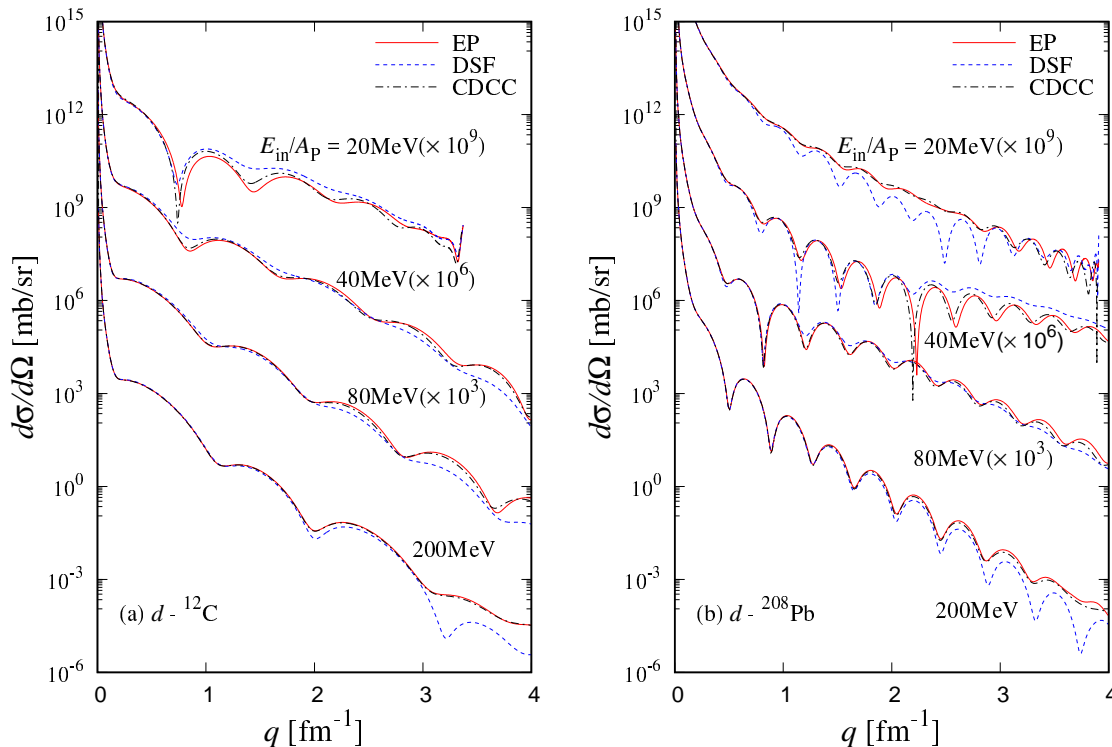


FIG. 1: Differential cross sections $d\sigma/d\Omega$ as a function of transfer momentum q for d scattering from (a) ^{12}C and (b) ^{208}Pb targets at $E_{\text{in}}/A_{\text{P}} = 20\text{--}200$ MeV. The solid line represents the result of the EP model, the dashed line denotes the result of the DSF model, and the dot-dashed line corresponds to the result of CDCC, respectively. Each cross section is multiplied by the factor shown in the figure.

center-of-mass (c.m.) motion is removed with the standard procedure [9]. For ^{12}C , we take the phenomenological proton-density determined from electron scattering [36]; here the finite-size effect of proton charge is unfolded with the standard procedure [37], and the neutron density is assumed to have the same geometry as the proton one.

III. RESULTS AND DISCUSSIONS

A. differential cross section for d scattering

We investigate d scattering from ^{12}C and ^{208}Pb targets at $E_{\text{in}}/A_{\text{P}} = 20\text{--}200$ MeV by using the DSF model, the EP model, and CDCC. It is known that CDCC has been successful in analyses of d scattering [1], so we regard CDCC as the exact calculation in this study.

Figure 1 shows the q dependence of $d\sigma/d\Omega$ for d scattering from (a) ^{12}C target and (b) ^{208}Pb target at the incident energies $E_{\text{in}}/A_{\text{P}} = 20\text{--}200$ MeV. The dashed and dotted lines stand for the results of the DSF model and CDCC, respectively. The result of the EP model is shown by the solid line. The difference between the

dashed and dotted lines represents breakup effects of d on the elastic scattering that become more important at forward angles as the incident energy decreases. One sees that the EP model well reproduces the results of CDCC for both ^{12}C and ^{208}Pb targets for $E_{\text{in}}/A_{\text{P}} \geq 80$ MeV. For $E_{\text{in}}/A_{\text{P}} \leq 40$ MeV, agreement between the EP model and CDCC is reasonably well although there is rather different behavior for the oscillation.

Here we consider the cause of the discrepancy between the EP model and CDCC for $E_{\text{in}}/A_{\text{P}} \leq 40$ MeV. The EP model includes the inaccuracy of the eikonal and adiabatic approximations because the EP model is based on the Glauber model. From the definition of the EP model, if we apply the eikonal approximation to the EP model, the obtained eikonal S matrix becomes the same as S_{N} of the Glauber model. This means that the EP model might be regarded as the Glauber model without the eikonal approximation, i.e. the calculation with only the adiabatic approximation. To clear this point, we calculate the differential cross section for d scattering by the Glauber model and CDCC with the adiabatic approximation (adiabatic-CDCC). In adiabatic-CDCC, energies for all excited states are replaced by the ground-state energy.

Figure 2 shows the results of the EP model, the Glauber model, and adiabatic-CDCC for d scattering

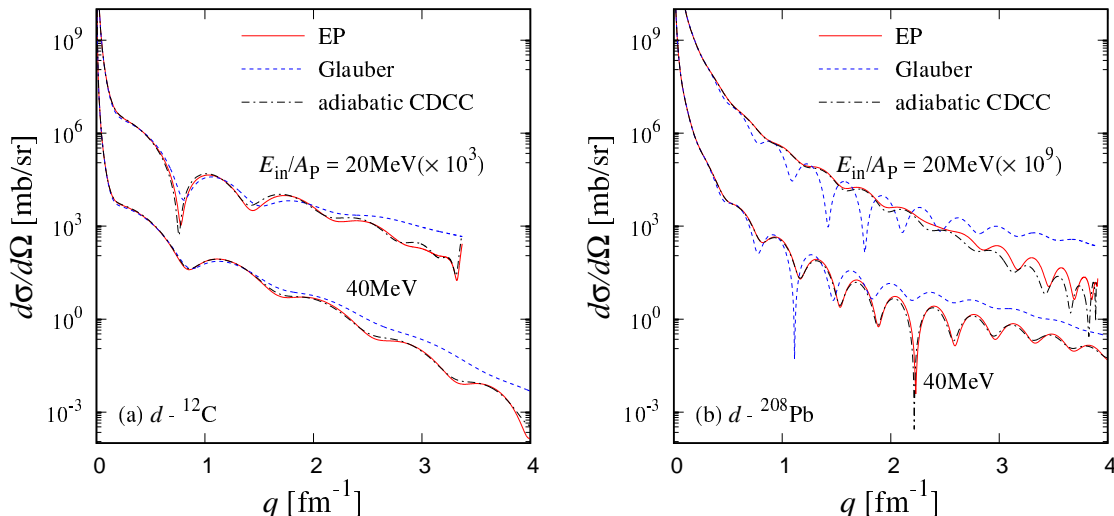


FIG. 2: Differential cross sections $d\sigma/d\Omega$ as a function of transfer momentum q for d scattering from (a) ^{12}C and (b) ^{208}Pb target at $E_{\text{in}}/A_{\text{P}} = 20\text{--}40$ MeV. The solid line represents the result of the EP model, the dashed line denotes the result of the Glauber model, and the dot-dashed line corresponds to the result of adiabatic-CDCC, respectively. Each cross section is multiplied by the factor shown in the figure.

from the ^{12}C target (a) and the ^{208}Pb target (b) at $E_{\text{in}}/A_{\text{P}} \leq 40$ MeV. The solid, dashed, and dot-dashed lines represent the results of the EP model, the Glauber model, and adiabatic-CDCC, respectively. One sees that the difference between the Glauber model and adiabatic-CDCC is not negligible. This means that the eikonal approximation is inaccurate because of the low-energy scattering. In particular, the results of the Glauber model are significantly different from those of adiabatic-CDCC for d scattering from ^{208}Pb . The reason is that the Coulomb interaction cannot be treated precisely in the eikonal approximation in addition to the low-energy scattering. On the other hand, the EP model simulates well the results of adiabatic-CDCC. This result shows that the discrepancy between the EP model and CDCC shown in Fig. 1 represents mainly the inaccuracy of the adiabatic approximation. Thus we conclude that the inaccuracy of the eikonal approximation in the EP model is partially excluded.

B. differential cross section of ^6He scattering

Next we apply the EP model to analyses of $^6\text{He} + ^{12}\text{C}$ scattering, which is described as a $^4\text{He} + n + n + \text{T}$ four-body model. As the exact calculation for the four-body scattering system, we adopt four-body CDCC that has been successful in analyses of breakup reaction of ^6He [38–40]. In the EP model for the four-body system, the eikonal S matrix defined in Eq. (16) is rewritten by

$$S_{\text{N}}(\mathbf{b}) = \langle \Phi_0 | e^{i\chi_{\text{N}}(\boldsymbol{\xi}, \mathbf{b})} | \Phi_0 \rangle, \quad (27)$$

and the phase-shift function is defined as

$$\chi_{\text{N}}(\boldsymbol{\xi}, \mathbf{b}) = -\frac{1}{\hbar v} \int_{-\infty}^{\infty} U(\boldsymbol{\xi}, \mathbf{R}) dZ \quad (28)$$

with

$$U(\boldsymbol{\xi}, \mathbf{R}) = U_n(\boldsymbol{\xi}, \mathbf{R}) + U_n(\boldsymbol{\xi}, \mathbf{R}) + U_\alpha(\boldsymbol{\xi}, \mathbf{R}). \quad (29)$$

Here $\boldsymbol{\xi}$ represents the internal coordinate of ^6He , and U_n (U_α) is the optical potential between n (^4He) and T. For U_n , we use the same potential used in the analysis of d scattering, and U_α is obtained by folding U_n and U_p with the ^4He density. The ground state wave function of ^6He , Φ_0 , is calculated by the Gaussian expansion method (GEM) with a $^4\text{He} + n + n$ three-body model. In GEM, the model Hamiltonian of ^6He and the parameter set of the Gaussian basis functions are adopted the same ones used in Ref. [41].

Figure 3 shows the results of the EP model (the solid line), the DSF model (the dotted line), and CDCC (the dot-dashed line) for the ^6He scattering from ^{12}C at $E_{\text{in}}/A_{\text{P}} = 20\text{--}200$ MeV. One sees that breakup effects of ^6He represented by the difference between the results of the DSF model and CDCC are stronger than those of d . Furthermore the EP model well reproduces the results of CDCC even at $E_{\text{in}}/A_{\text{P}} \leq 40$ MeV. One of the reason is that the condition represented by Eq. (9) is satisfied well because K of the ^6He scattering is larger than K of the d scattering in the same $E_{\text{in}}/A_{\text{P}}$. Thus we expect that the EP model works well for scattering with heavier projectiles.

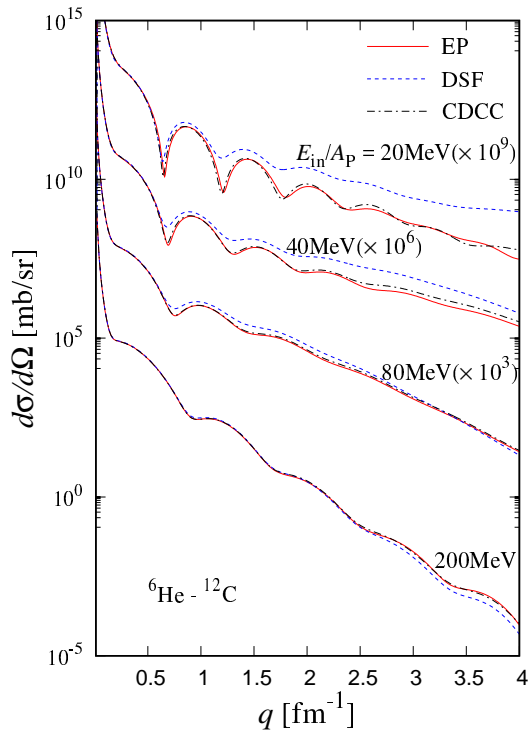


FIG. 3: The same as Fig. 1, but for ${}^6\text{He}$ scattering from ${}^{12}\text{C}$ at $E_{\text{in}}/A_{\text{P}} = 20\text{--}200$ MeV.

C. dynamical polarization potential

Finally, we discuss breakup effects of the optical potential for the ${}^6\text{He}$ scattering. Figure 4 shows the optical potentials derived by the EP model and the DSF model for ${}^6\text{He}$ scattering from ${}^{12}\text{C}$ at $E_{\text{in}}/A_{\text{P}} = 40$ MeV. The solid line represents the eikonal potential, and the dashed line corresponds to the DSF potential that doesn't include breakup effects of ${}^6\text{He}$. The dot-dashed line stands for the dynamical polarization (DP) potential U_{DP} defined as

$$U_{\text{DP}}(R) = U_{\text{E}}(R) - U_{\text{DSF}}(R), \quad (30)$$

which represents breakup effects of ${}^6\text{He}$ on the optical potential between ${}^6\text{He}$ and ${}^{12}\text{C}$. In this figure, the strength of the DP potential is multiplied by 2.

In Fig. 4, the real part of the DP potential is repulsive in the peripheral region and the imaginary part is absorptive in the whole region. This behavior of the DP potential can be understood from the S matrices for the scattering. In the eikonal approximation as shown in Eqs. (27) and (28), the real part of the optical potential is related to the argument of the S matrix, and the imaginary part of the optical potential is the absolute value of the S matrix. Figure 5 shows the S matrices for the scattering. The cross, circle and square marks stand for the results of the EP model, the DSF model, and CDCC, respectively.

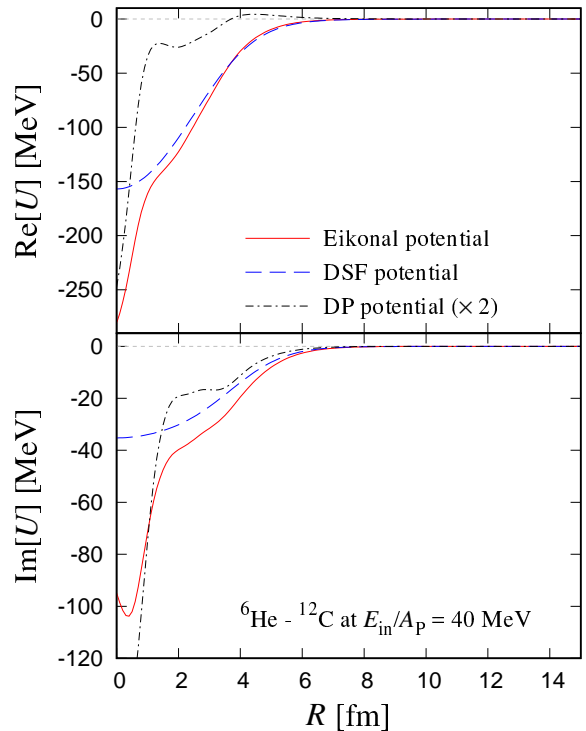


FIG. 4: The R dependence of the potentials for ${}^6\text{He}$ scattering from ${}^{12}\text{C}$ at $E_{\text{in}}/A_{\text{P}} = 40$ MeV. The solid and dashed lines represent the eikonal potential and the DSF potential. The dot-dashed line stands for the dynamical polarization potential and is multiplied by 2.

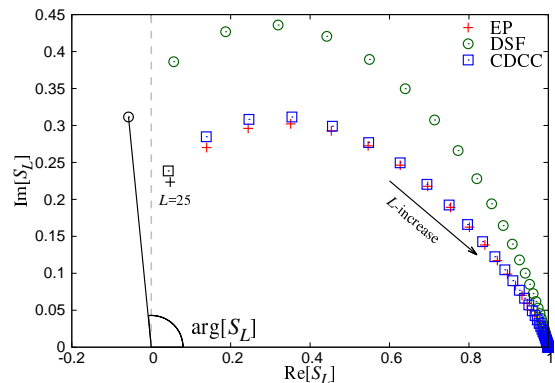


FIG. 5: The S matrices for ${}^6\text{He}$ scattering from ${}^{12}\text{C}$ at $E_{\text{in}}/A_{\text{P}} = 40$ MeV are plotted from the grazing angular momentum. The cross, circle, square points describe the results of the EP model, the DSF model, CDCC, respectively. L means the orbital angular momentum, and increases toward the $S = (1, 0)$.

CDCC, respectively. The S matrices are plotted from the grazing angular momentum $L = 25$, which is defined this momentum as a position of the peak at the partial breakup cross section. The difference between the results of the DSF model and CDCC represents breakup effects on the S matrix, and the results of the EP model are in good agreement with those of CDCC. One sees that the absolute value of the S matrix for CDCC is smaller than that for the DSF model, and the argument of the S matrix for CDCC is also smaller than that for the DSF model. This result shows that breakup effects make weak for the real part and strong for the imaginary part of the optical potential.

IV. SUMMARY

We construct a microscopic optical potential including breakup effects based on the Glauber model, in which a NA potential is derived by the folding model with the Melbourne g matrix. The microscopic optical potential is referred to as the eikonal potential.

First, in order to confirm the validity of the eikonal potential, we compared the EP model with CDCC for the elastic cross sections for d scattering from ^{12}C and ^{208}Pb at $E_{\text{in}}/A_{\text{P}} = 20\text{--}200$ MeV, where the scattering system is described by the $p + n + \text{T}$ three-body model. As the result, the EP model well reproduces the results of CDCC as the incident energy increases. In the analysis, we found that the difference between the results of the EP model and CDCC at low incident energies comes from mainly the inaccuracy of the adiabatic approximation, and the inaccuracy of the eikonal approximation is

partially excluded from the EP model. In fact, the EP model simulates well the result of adiabatic-CDCC for $E_{\text{in}}/A_{\text{P}} \leq 40$ MeV.

Next, we apply the EP model to analyses of ^6He scattering from ^{12}C at $E_{\text{in}}/A_{\text{P}} = 20\text{--}200$ MeV, where the scattering system is described by a $^4\text{He} + n + n + ^{12}\text{C}$ four-body model. In the analyses of ^6He scattering, the EP model well reproduces the results of CDCC even at $E_{\text{in}}/A_{\text{P}} \leq 40$ MeV. This means that because the wave number of the ^6He scattering is larger than that of the d scattering in the same $E_{\text{in}}/A_{\text{P}}$, the eikonal approximation is valid even at $E_{\text{in}}/A_{\text{P}} \leq 40$ MeV. Thus the EP model works well for heavier projectile scattering. Furthermore we investigated breakup effects on the optical potential via the dynamical polarization potential.

One of the advantage of the EP model is to be applicable to analyses for scattering of many-body projectiles as well as the Glauber model. In the forthcoming paper, we will try to apply the EP model to analyses of scattering of ^8He , in which ^8He is described by a $^4\text{He} + n + n + n + n$ five-body model. Furthermore, we will discuss Coulomb breakup effects, which are omitted in the present calculation. The treatment of Coulomb breakup processes within the eikonal approximation has been discussed in some papers [42, 43], and the problem is an important subject for the eikonal calculation.

Acknowledgements

This work is supported in part by by Grant-in-Aid for Scientific Research (Nos. 25400266, and 26400278) from Japan Society for the Promotion of Science (JSPS).

-
- [1] M. Kamimura, M. Yahiro, Y. Iseri, Y. Sakuragi, H. Kameyama, and M. Kawai, Prog. Theor. Phys. Suppl. **89**, 1 (1986).
 - [2] N. Austern, Y. Iseri, Y. Sakuragi, M. Kawai, G. Rawitscher, and M. Yahiro, Phys. Rep. **154**, 125 (1987).
 - [3] M. Yahiro, K. Ogata, T. Matsumoto, and K. Minomo, Prog. Theor. Exp. Phys. (2012) 01A206.
 - [4] H. F. Arellano, F. A. Brieva, and W. G. Love, Phys. Rev. C **52**, 301 (1995).
 - [5] K. Minomo, K. Ogata, M. Kohno, Y. R. Shimizu, and M. Yahiro, J. Phys. G **37**, 085011 (2010)
 - [6] B. Sinha, Phys. Rep. **20**, 1 (1975).
B. Sinha and S. A. Moszkowski, Phys. Lett. **B81**, 289 (1979).
 - [7] D. T. Khoa, W. von Oertzen, H. G. Bohlen, and S. Ohkubo, J. Phys. G **34**, R111 (2007).
 - [8] T. Furumoto, Y. Sakuragi, and Y. Yamamoto, Phys. Rev. C **82**, 044612 (2010).
 - [9] T. Sumi, K. Minomo, S. Tagami, M. Kimura, T. Matsumoto, K. Ogata, Y. R. Shimizu, and M. Yahiro, Phys. Rev. C **85**, 064613 (2012).
 - [10] G. Bertsch, J. Borysowicz, H. McManus, and W. G. Love, Nucl. Phys. A **284**, 399 (1977).
 - [11] J. -P. Jeukenne, A. Lejeune, and C. Mahaux, Phys. Rev. C **16**, 80 (1977);
J. -P. Jeukenne, A. Lejeune, and C. Mahaux, Phys. Rep. **25**, 83 (1976).
 - [12] F. A. Brieva and J. R. Rook, Nucl. Phys. A **291**, 299 (1977); *ibid.* 291, 317 (1977); *ibid.* 297, 206 (1978).
 - [13] G. R. Satchler and W. G. Love, Phys. Rep. **55**, 183 (1979).
 - [14] G. R. Satchler, "Direct Nuclear Reactions", Oxford University Press, (1983).
 - [15] N. Yamaguchi, S. Nagata, and T. Matsuda, Prog. Theor. Phys. **70**, 459 (1983); N. Yamaguchi, S. Nagata, and J. Michiyama, Prog. Theor. Phys. **76**, 1289 (1986).
 - [16] L. Rikus, K. Nakano, and H. V. Von Geramb, Nucl. Phys. A **414**, 413 (1984); L. Rikus, and H. V. Von Geramb, Nucl. Phys. A **426**, 496 (1984).
 - [17] K. Amos, P. J. Dortmans, H. V. Von Geramb, S. Karataglidis, and J. Raynal, in *Advances in Nuclear Physics*, edited by J. W. Negele and E. Vogt (Plenum, New York, 2000) Vol. 25, p. 275.
 - [18] S. M. Saliem and W. Haider, J. Phys. G **28**, 1313 (2002).
 - [19] T. Furumoto, Y. Sakuragi, and Y. Yamamoto, Phys. Rev. C **78**, 044610 (2008); *ibid.*, **79**, 011601(R) (2009); *ibid.*,

- 80**, 044614 (2009).
- [20] M. Toyokawa, M. Yahiro, T. Matsumoto, K. Minomo, K. Ogata and M. Kohno, *Phys. Rev. C* **92**, 024618 (2015).
- [21] K. Egashira, K. Minomo, M. Toyokawa, T. Matsumoto and M. Yahiro, *Phys. Rev. C* **89**, 064611 (2014).
- [22] M. Toyokawa, T. Matsumoto, K. Minomo and M. Yahiro, *Phys. Rev. C* **91**, 064610 (2015).
- [23] K. M. Watson, *Phys. Rev.* **89**, 575 (1953).
- [24] A. K. Kerman, H. McManus, and R. M. Thaler, *Ann. Phys.* **8**, 551 (1959).
- [25] M. Yahiro, K. Minomo, K. Ogata, and M. Kawai, *Prog. Theor. Phys.* **120**, 767 (2008).
- [26] R. J. Glauber, in *Lectures in Theoretical Physics*, edited by W. E. Brittin (Interscience, New York, 1959), Vol. **1**, pp 315–414.
- [27] K. Yabana, Y. Ogawa, and Y. Suzuki, *Phys. Rev. C* **45**, 2909 (1992).
- [28] B. Abu-Ibrahim and Y. Suzuki, *Phys. Rev. C* **62**, 034608 (2000).
- [29] T. Ohmura, B. Imanishi, M. Ichimura, and M. Kawai, *Prog. Theor. Phys.* **43**, 347 (1970).
- [30] Y. C. Tang, M. LeMere, and D. R. Thompson, *Phys. Rep.* **47**, 167 (1978).
- [31] K. Aoki and H. Horiuchi, *Prog. Theor. Phys.* **69**, 857 (1983), and references therein.
- [32] J. W. Negele and D. Vautherin, *Phys. Rev. C* **5**, 1472 (1972).
- [33] R. Machleidt, K. Holinde, and Ch. Elster, *Phys. Rep.* **149**, 1 (1987).
- [34] M. Toyokawa, K. Minomo, and M. Yahiro, *Phys. Rev. C* **88**, 054602 (2013).
- [35] J. F. Berger, M. Girod, and D. Gogny, *Comput. Phys. Commun.* **63**, 365 (1991).
- [36] H. de Vries, C. W. de Jager, and C. de Vries, *At. Data Nucl. Data Tables* **36**, 495 (1987).
- [37] R. P. Singhal, M. W. S. Macauley, and P. K. A. De Witt Huberts, *Nucl. Instrum. and Method* **148**, 113 (1978).
- [38] T. Matsumoto, E. Hiyama, K. Ogata, Y. Iseri, M. Kamimura, S. Chiba, and M. Yahiro, *Phys. Rev. C* **70**, 061601(R) (2004).
- [39] T. Matsumoto, T. Egami, K. Ogata, Y. Iseri, M. Kamimura, and M. Yahiro, *Phys. Rev. C* **73**, 051602(R) (2006).
- [40] M. Rodríguez-Gallardo, J. M. Arias, J. Gómez-Camacho, R. C. Johnson, A. M. Moro, I. J. Thompson, and J. A. Tostevin, *Phys. Rev. C* **77**, 064609 (2008).
- [41] Y. Kikuchi, T. Matsumoto, M. Kosho, and K. Ogata, *Phys. Rev. C* **88**, 021602 (2013).
- [42] K. Ogata, M. Yahiro, Y. Iseri, T. Matsumoto, and M. Kamimura, *Phys. Rev. C* **68**, 064609 (2003).
- [43] P. Capel, D. Baye, and Y. Suzuki, *Phys. Rev. C* **78**, 054602 (2008).